IEEE Access
Multidisciplinary | Rapid Review | Open Access Journal

Received November 11, 2020, accepted November 12, 2020, date of publication November 17, 2020,
date of current version November 30, 2020.

Digital Object Identifier 10.1109/ACCESS.2020.3038449

Accuracy and Error Analysis of Vector Measurement of Ocean Surface Current by Multi-Aperture Along-Track Interferometric SAR

YAN LI[1,2,3], JINSONG CHONG[1,2], (Senior Member, IEEE), KAI SUN[1,2,3], XUE YANG[1,2,3], AND YAWEI ZHAO[1,2,3]

[1]Aerospace Information Research Institute, Chinese Academy of Sciences, Beijing 100190, China
[2]National Key Lab of Microwave Imaging Technology, Beijing 100190, China
[3]School of Electronics, Electrical and Communication Engineering, University of Chinese Academy of Sciences, Beijing 100049, China

Corresponding author: Jinsong Chong (iecas_chong@163.com)

ABSTRACT The ocean surface current vector contains velocity and direction information, and its acquisition method has important research value in marine applications. Multi-aperture along-track interferometric (MA-ATI) SAR is a novel method of current vector detection. However, due to the lack of real experimental data validation, complex marine environment and diverse system parameters have an uncertain impact on the current measurement ability of MA-ATI SAR. Therefore it is necessary to analyze the measurement accuracy and error of this method in theory. Based on the current measurement principle of MA-ATI SAR, this article deduces and establishes the accuracy and error simulation model, and analyzes the influence of radar parameters and marine environment on the velocity and direction results. In the simulation results, the airborne MIMO-SAR radar parameters is more suitable to use MA-ATI method for accurate current measurement, and the accuracy of current measurement is higher for the current with high velocity and direction close to azimuth. It is found that the variation of wind direction will lead to obvious errors in MA-ATI current results, and it is pointed out that accurate current results can be obtained by iteratively correcting the velocity error of sub-apertures using M4S model.

INDEX TERMS Multi-aperture along-track interferometric (MA-ATI), current vector, current measurement accuracy, current measurement error.

I. INTRODUCTION

In 1987, Goldstein and Zebker proposed the Along-Track Interferometric SAR (ATI-SAR) technology [1], which provided the possibility of retrieving large-scale and high-resolution ocean surface current fields. ATI-SAR uses two antennas installed along the azimuth direction to separately image the ocean surface. Due to the imaging time difference and the movement of the ocean surface scatterers, there is phase difference between the two single look complex (SLC) images, which is named the interferometric phase. The interferometric phase is proportional to the ocean surface velocity in the radar line-of-sight direction, so the traditional ATI-SAR can only measure the range velocity component of the current, and it is difficult to retrieve current vectors.

In order to measure the high-resolution ocean current vectors, the ATI-SAR results of two sets of flight trajectories can be used for synthesis, but only the currents in the area where the trajectories overlap can be obtained [2]. The Dual-Beam Interferometry (DBI) technology proposed by Frasier and Camps [3] in 2001 achieved the goal of measuring the current vectors within the entire swath in a single flight. However, since the system requires four antennas and the hardware design is complicated, there are only reports on airborne verification experiments [4], and the spaceborne dual-beam system is under research and design [5]. Different from the research status of DBI, ATI-SAR has obtained a large amount of airborne and spaceborne data. Therefore,

The associate editor coordinating the review of this manuscript and approving it for publication was Haiyong Zheng.

Ouchi *et al.* [6], [7] innovatively proposed the Multi-Aperture Along-Track Interferometric (MA-ATI) SAR method using existing ATI-SAR data for current vector measurements, which performs sub-aperture processing on ATI-SAR data to estimate current directions, and combine with the range current velocity components measured by ATI-SAR to acquire the current vectors. However, there is only a feasibility simulation verification study on this method [8], and it has not been applied to actual data processing.

Considering that the abundant airborne and spaceborne ATI-SAR data has many different radar parameters, such as baseline length, the incidence angle, the sub-aperture squint angle, etc., and the wind and current in the environment are constantly changing, the influence of these factors on the MA-ATI results is not yet clear. Therefore, it is necessary to theoretically evaluate the measurement performance before the application of MA-ATI, including analysis of the accuracy and error of current measurements.

In this article, based on the principle of MA-ATI, the accuracy and error model of current measurements are derived. The effects of different radar parameters and current parameters on the accuracy of velocity and direction are simulated and analyzed. Then, it analyzes the current vector measurement errors caused by the wind field, and finally gives an error correction method. These contents provides guidance for the future processing and application of MA-ATI method in actual data.

II. MA-ATI CURRENT MEASUREMENT ACCURACY AND ERROR MODEL

A. BRIEF INTRODUCTION OF MA-ATI PRINCIPLE

In order to facilitate the discussion of current measurement accuracy and error model later, this article first briefly describes the principle of MA-ATI based on the literature [6]–[8]. It should be pointed out that, in order to make the expression of this article more convenient and consistent, the content of this section adopts different expressions for certain variables, and explains all variables under the premise of fully respecting the basic principles of MA-ATI.

In the traditional ATI-SAR technology, the interferometric phase ϕ is obtained by conjugate multiplication of the full-aperture SLC images A_f and A_a obtained by the fore and aft antennas separately [9].

$$\phi_r = \arctan\left(\frac{imag\left(A_f A_a^*\right)}{real\left(A_f A_a^*\right)}\right) = \frac{4\pi}{\lambda} u_r \sin\theta_i \cdot \Delta t \qquad (1)$$

where $imag(\cdot)$ and $real(\cdot)$ represent the operation of taking the imaginary and real part of the complex data respectively, the asterisk indicates the conjugate of complex data, λ represents the signal wavelength, u_r represents the range velocity component of the current, θ_i represents the incidence angle and Δt represents the imaging time interval, which is related to the platform speed and the effective baseline length. In the standard mode of single-transmit and dual-receive antennas, the effective baseline length is half of the physical baseline length. In the ping-pong mode of dual-transmit and dual-receive antennas, the effective baseline length is equal to the physical baseline length. From (1), only one-dimensional current field can be retrieved, and it is difficult to obtain the current vectors.

At first ATI is used to obtain the range velocity component of current, and then MA-ATI performs azimuth sub-aperture processing on the SAR data acquired by the fore-and-aft antennas to obtain four sub-aperture SLC data, two of which represent the forward looking results with a small squint angle, and the other two represent the backward looking results with the same squint angle. The geometric relationship of the MA-ATI system is shown in Figure 1 [6], [7], where B represents the baseline length. The two SLC images of the forward direction are processed by interference processing to obtain the forward-looking interferometric phase and the forward velocity component of current. The same processing obtains the backward-looking interferometric phase and the backward velocity component. The current direction can be directly obtained from the interferometric phase, or indirectly from the forward and backward velocity components [7]. The geometric relationship between the current vector and its various velocity components is shown in Figure 2 [6]–[8].

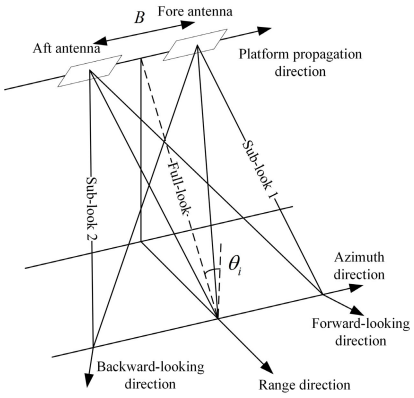

FIGURE 1. MA-ATI system geometric diagram [6], [7].

In Figure 2, u represents the observed current vector, u_a, u_r, u_f and u_b respectively represent the velocity components of the current in the azimuth, range, forward and

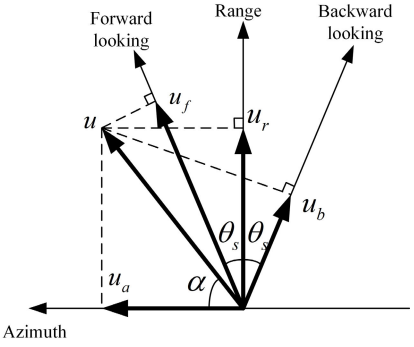

FIGURE 2. The schematic diagram of the geometric relationship between the current vector and its components [6]–[8].

backward directions, θ_s is the sub-aperture squint angle after sub-aperture processing, which is proportional to the azimuth beam width, and α is the angle between the current vector and the azimuth direction, which defines the current direction, and is an important parameter to be sought. According to the geometric description in Figure 2, we can get [6]

$$u_f = u\cos\left(\pi/2 - \alpha - \theta_s\right) = u\sin\left(\alpha + \theta_s\right) \tag{2}$$

$$u_b = u\cos\left(\pi/2 - \alpha + \theta_s\right) = u\sin\left(\alpha - \theta_s\right) \tag{3}$$

By subtracting (2) and (3), azimuth velocity component u_a can be obtained

$$u_a = \frac{u_f - u_b}{2\sin\theta_s} \tag{4}$$

and then it shows the current direction α

$$\alpha = \arctan\left(\frac{u_r}{u_a}\right) = \arctan\left(\frac{2u_r\sin\theta_s}{u_f - u_b}\right) \tag{5}$$

Ouchi *et al.* [7], [9] pointed out that the MA-ATI is similar to the multi-aperture interferometry (MAI) method using cross-track differential interferometric SAR to measure two-dimensional deformation, and the effectiveness of MAI has been verified by experiments [10], [11]. Therefore, MA-ATI should also be feasible in practice [9]. In addition, Yoshida *et al.* [8] verified the effectiveness of MA-ATI in estimating ocean surface directions through time domain signal simulation, but only analyzed the results of a group of airborne parameters under different sub-aperture squint angles, and pointed out that it is necessary to carry out simulation under more parameters before actual data processing. Therefore, this article analyzes the accuracy and error of MA-ATI current measurements, and simulates the results under different system and environmental parameters.

B. CURRENT MEASUREMENT ACCURACY MODEL OF MA-ATI

For the traditional ATI-SAR method, the accuracy of range velocity component of the current is expressed by the standard deviation of this variable [12],

$$\sigma_{u_r} = \frac{v_p\lambda}{4\pi B_{eff}\sin\theta_i}\sigma_{\phi_r} \tag{6}$$

where v_p is the speed of platform, λ is the signal wavelength, B_{eff} is the effective baseline length, and σ_{ϕ_r} is the interferometric phase accuracy, which can be expressed as [12], [13]

$$\sigma_{\phi_r} = \sqrt{\frac{1-\gamma^2}{2N\gamma^2}} \tag{7}$$

where N is the number of looks in each complex image, expressed as [12]

$$N = \rho_{L2}/\rho_{2D} \tag{8}$$

where ρ_{L2} represents the product resolution of current field, ρ_{2D} represents the system geometric resolution, that is, the product of azimuth and range resolution. γ is the coherence coefficient of the interferogram, which is mainly composed of three parts [12],

$$\gamma = \gamma_{SNR}\cdot\gamma_t\cdot\gamma_{sys} \tag{9}$$

where γ_{SNR} is the signal-to-noise ratio decoherence, γ_t is the time decoherence caused by random ocean surface motion, and they are respectively expressed as [12]

$$\gamma_{SNR} = 1\Big/\left(1 + SNR^{-1}\right) \tag{10}$$

$$\gamma_t = \exp\left(-\Delta t^2\Big/\tau_c^2\right) \tag{11}$$

where SNR is the signal-to-noise ratio, Δt is the imaging time interval, and τ_c is the ocean surface coherence time, which decreases with the increase of radar frequency and wind speed. γ_{sys} is the system decoherence caused by ambiguities and quantization, which is usually very small [12].

According to the literature [14], [15], the standard deviation of the forward- and backward-looking interferometric phase after sub-aperture processing can be expressed as

$$\sigma_{\phi_f} = \sigma_{\phi_b} = \sqrt{\frac{1-\gamma^2}{N\gamma^2}} \tag{12}$$

Therefore, the measurement accuracy σ_{u_f} of the forward velocity component and σ_{u_b} of the backward velocity component can be expressed as

$$\sigma_{u_f} = \frac{v_p\lambda}{4\pi B_{eff}\sin\theta_i}\sigma_{\phi_f} \tag{13}$$

$$\sigma_{u_b} = \frac{v_p\lambda}{4\pi B_{eff}\sin\theta_i}\sigma_{\phi_b} \tag{14}$$

Combining (12)-(14) with (4), and according to the error transfer formula, this article derives the measurement accuracy σ_{u_a} of the azimuth velocity component in MA-ATI, expressed as

$$\sigma_{u_a} = \sqrt{\frac{\sigma_{u_f}^2 + \sigma_{u_b}^2}{(2\sin\theta_s)^2}} = \frac{v_p\lambda}{4\pi B_{eff}\sin\theta_i\sin\theta_s}\sqrt{\frac{1-\gamma^2}{2N\gamma^2}} \tag{15}$$

Furthermore, the vector velocity measurement accuracy σ_u is

$$\sigma_u = \sqrt{\sigma_{u_a}^2 + \sigma_{u_r}^2} = \frac{v_p\lambda}{4\pi B_{eff}\sin\theta_i\sin\theta_s}\sqrt{\frac{\left(1-\gamma^2\right)\left(1+\sin^2\theta_s\right)}{2N\gamma^2}} \tag{16}$$

According to the error transfer formula, this article further derives the direction measurement accuracy σ_α of the MA-ATI as

$$\sigma_\alpha = \sqrt{\left(\frac{\partial\alpha}{\partial u_r}\right)^2\sigma_{u_r}^2 + \left(\frac{\partial\alpha}{\partial u_a}\right)^2\sigma_{u_a}^2} \tag{17}$$

where

$$\frac{\partial \alpha}{\partial u_r} = \frac{1}{1+\left(u_r/u_a\right)^2} \cdot \frac{1}{u_a} = \frac{u_a}{u_a^2+u_r^2} = \frac{\cos(\alpha)}{u} \tag{18}$$

$$\frac{\partial \alpha}{\partial u_a} = \frac{1}{1+\left(u_r/u_a\right)^2} \cdot \left(-\frac{u_r}{u_a^2}\right) = \frac{u_r}{u_a^2+u_r^2} = \frac{\sin(\alpha)}{u} \tag{19}$$

It should be noted that, since the current direction is a nonlinear function, when the error of the independent variable is small, the tangent line can be approximately used to obtain the function error, otherwise the error transfer formula cannot be applied. Therefore, when the calculated value of (17) is small, it is credible. If the calculated value σ_α exceeds 180 ° or even greater, it can only show that the error is very large, and the practical significance is not considered.

According to the above analysis and deduced model formulas, it can be seen that the measurement accuracy of the current vector will be affected by radar parameters such as baseline length, incidence angle, and sub-aperture squint angle. The direction measurement accuracy is also related to the change of the measured current vector.

C. CURRENT MEASUREMENT ERROR MODEL OF MA-ATI

In the actual interferometric data processing process, the range velocity u_r obtained by interferometric phase includes not only the ocean surface current velocity u_C, but also the net Bragg wave phase velocity u_B and the large-scale wave orbit velocity u_O [16]:

$$u_r = u_C + u_B + u_O \tag{20}$$

It is generally considered that the large-scale wave orbit velocity is periodic along the wave propagation direction and the mean value is zero [17], [18]. Therefore, the orbital velocity component can be removed by spatial average. Romeiser *et al.* [19] processed the orbital velocity component of TanDEM-X SAR data by spatial averaging, and retrieved satisfied current field results. However, it should be pointed out that there will be a small amount of residual orbital velocity under the complex ocean conditions when the current direction does not satisfy the isotropy. For the sake of simplicity, this article does not consider the deviation caused by orbital velocity, and more research on orbital velocity can refer to references [18], [20]. Therefore, the net Bragg wave phase velocity is the main factor causing the deviation of current, and it is also the cause of the current measurement error in MA-ATI discussed in this article.

Studies have shown that the echo signal usually contains two Bragg wave phase velocities $\pm c_p$ with opposite propagation directions, expressed as [18], [21], [22]:

$$c_p = \sqrt{\frac{g}{k_b} + \frac{\tau_s \cdot k_b}{\rho}} \tag{21}$$

where g is the acceleration of gravity, τ_s is the ocean surface tension, ρ is the density of seawater, and k_b is the magnitude of the Bragg wavenumber, which is related to the electromagnetic wavenumber k_e and the incidence angle θ_i:

$$k_b = 2k_e \sin\theta_i \tag{22}$$

The respective proportions of the two Bragg wave phase velocities with opposite propagation directions are related to the angle θ_w between the wind direction and the radar looking direction, and also related to the direction expansion function G [3], [18]:

$$G(\theta_w) = \cos^{2n}\left(\theta_w/2\right) \tag{23}$$

where n is the expansion factor, which is generally taken as from 2 to 5. According to the discussion in the related literature [3], [18], the simulation in this article takes the value of n as 3. Therefore, the net Bragg phase velocity u_B in the actual data resolution unit is expressed as [18]:

$$u_B = \frac{G(\theta_w) - G(\theta_w+\pi)}{G(\theta_w) + G(\theta_w+\pi)} c_p \tag{24}$$

Equation (24) represents the measurement deviation affected by the angle between the wind direction and the radar looking direction in the marine environment.

Based on the analysis of the previous studies above, this article expresses the forward velocity component error ε_{u_f} obtained from the forward-looking sub-aperture and the backward velocity component error ε_{u_b} obtained from the backward-looking sub-aperture as

$$\varepsilon_{u_f} = \frac{G(\theta_w+\theta_s) - G(\theta_w+\theta_s+\pi)}{G(\theta_w+\theta_s) + G(\theta_w+\theta_s+\pi)} c_p \tag{25}$$

$$\varepsilon_{u_b} = \frac{G(\theta_w-\theta_s) - G(\theta_w-\theta_s+\pi)}{G(\theta_w-\theta_s) + G(\theta_w-\theta_s+\pi)} c_p \tag{26}$$

Combining (4) to derive the azimuth velocity component error ε_{u_a} caused by wind direction as

$$\varepsilon_{u_a} = \frac{\varepsilon_{u_f} - \varepsilon_{u_b}}{2\sin\theta_s} \tag{27}$$

The range velocity component error ε_{u_r} is consistent with u_B expressed by (24). Furthermore, the current vector velocity error ε_u and the direction error ε_α are obtained:

$$\varepsilon_u = \sqrt{\left(u_a+\varepsilon_{u_a}\right)^2 + \left(u_r+\varepsilon_{u_r}\right)^2} - u \tag{28}$$

$$\varepsilon_\alpha = arc\tan\left(\frac{u_r+\varepsilon_{u_r}}{u_a+\varepsilon_{u_a}}\right) - \alpha \tag{29}$$

The current measurement error model of MA-ATI derived above shows that the change of wind direction will affect the actual measurement effect of MA-ATI.

III. SIMULATION ANALYSIS OF CURRENT VECTOR ACCURACY

A. ANALYSIS OF THE INFLUENCE OF RADAR PARAMETERS ON THE CURRENT VECTOR ACCURACY

In this article, the airborne parameters of PiSAR-L2 and MIMO-SAR, and spaceborne parameters of TerraSAR-X are selected for simulation analysis. The simulation parameters

TABLE 1. Simulation parameters of current measurement.

Parameters	PiSAR-L2	MIMO-SAR	TerraSAR-X	Unit
Radar Frequency f_c	1.2	5.4	9.6	GHz
Platform height H	6	2.06	514	Km
Platform speed v_p	200	105	7110	m/s
Resolution ρ	1	0.2	2	m
Incidence angle θ_i	40	40	40	deg
Sub-aperture squint angle θ_s	5	2	0.2	deg
Baseline length B_{eff}	0.47	0.15/0.3/0.45	1.2	m
Coherence time τ_c	60	20	10	ms

are shown in Table 1. PiSAR-L2 is a fully polarized airborne L-band system developed by Japan Aerospace Exploration Agency (JAXA) [23]. The parameters of PiSAR-L2 selected by us are consistent with those in reference [24]. MIMO-SAR is a high-resolution airborne SAR system developed by the Institute of Electronics, Chinese Academy of Sciences [25], which has three baseline lengths, and it has the multi-baseline along-track interferometric ability. TerraSAR-X is a SAR satellite with along-track interferometric mode and its current measurement capability has been verified in many documents [19], [26], [27].

Before the simulation, it is necessary to explain how to set the number of looks and correlation coefficient.The product resolution of the current field is assumed to be 1 km, so the number of looks can be calculated based on (8) with the resolution parameters of the three systems. For the designed system, the SNR of different data is variable, which increases with the increase of wind speed, decreases with the increase of platform height, and decreases with the increase of incidence angle within the swath. Therefore, after referencing the literature [3], [12], we set the SNR of 5dB, 10dB and 15dB to simulate. Then the decoherence caused by the SNR can be calculated according to (10).Time decoherence can be calculated using (11) based on baseline length, flight speed and ocean surface coherence time in Table 1, where coherence time is selected according to the discussion in [3]. The system decoherence is assumed to be 0.9, and the total coherence coefficient can be calculated from (9). It should be noted that although the radar frequencies of the three simulation parameters are different, the literature [28] shows that the radar frequency is not a key parameter for ATI. Therefore, the following mainly analyzes the influence of radar parameters on the current measurement accuracy from the baseline length, the incidence angle and the sub-aperture squint angle. In a uniform current field with a given velocity and direction, the current accuracy varies with the radar parameters in the same law. Therefore, unless otherwise specified, the current velocity of 1.77m/s and the direction of 45° are used for simulation by default, which is consistent with the parameters used in the literature [8].

The baseline length is an important parameter affecting the current measurement accuracy of ATI. Therefore, the variation of the current measurement accuracy with the baseline length is firstly studied in the case of three radar parameters. Figure 3 (a) shows the results of velocity

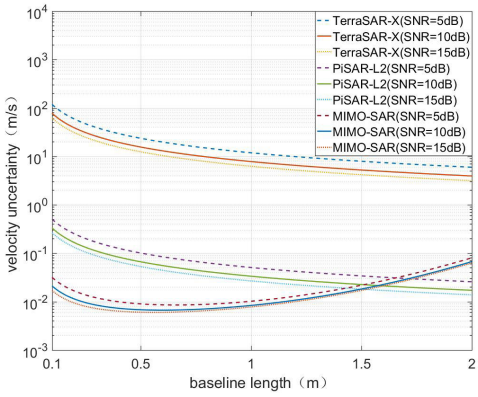

(a)

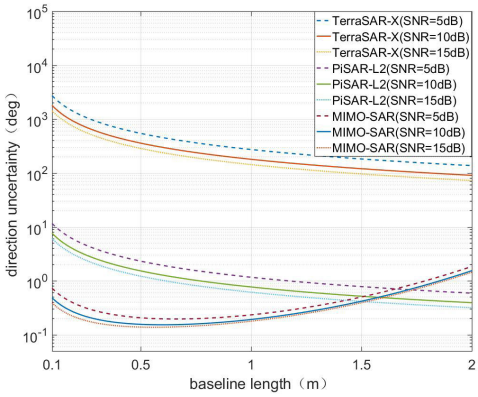

(b)

FIGURE 3. The accuracy of current vector varies with baseline length. (a) Change of velocity measurement accuracy. (b) Change of direction measurement accuracy.

measurement accuracy σ_u varying with baseline length simulated by (16), and figure 3 (b) shows the results of direction measurement accuracy σ_α with baseline length obtained from (17)-(19). According to the simulation results, it is obvious that the current measurement accuracy is higher with the higher signal-to-noise ratio. Secondly, the accuracy of the two airborne simulation results is better than that of the satellite TerraSAR-X simulation results, and the MIMO-SAR system has the highest measurement accuracy of velocity and direction. The MIMO-SAR system has the best results when the baseline length is 0.45 meters, and the current velocity accuracy reaches 0.007m/s and the direction accuracy reaches 0.16° when the SNR is 10dB. Therefore, the following simulation experiments on MIMO-SAR will be conducted under the condition of a baseline length of 0.45 meters. Within a variable baseline range of 2 meters, the accuracy of PiSAR-L2 and TerraSAR-X increases as the baseline length increases. If the variable baseline range is expanded, the optimal baseline length for PiSAR-L2 and TerraSAR-X systems can be found. The optimal baseline length of PiSAR-L2 is 11.4 meters with the highest velocity accuracy is 0.006m/s and the direction accuracy is 0.13° for 10dB SNR. The

optimal baseline length of TerraSAR-X is 20.3 meters, with which the velocity accuracy is 0.75m/s and the direction accuracy is 17.2° for 10dB SNR. According to the explanation of (17), this article considers that the simulation results under airborne parameters are generally small and reliable, while the results of spaceborne parameters are large and the practical application ability is low.

Figure 4 (a) and (b) shows the changes of current velocity and direction accuracy with the incidence angle, respectively. The results show that the larger the incidence angle, the higher the accuracy of the current vector. Among them, the results of TerraSAR-X are the worst, and the results of MIMO-SAR are the best. Within the range of medium incidence angles of 20° ∼ 70°, the current velocity accuracy of the MIMO-SAR is 0.005m/s ∼ 0.013m/s for 10dB SNR, and the direction accuracy is 0.1° ∼ 0.3°. It should be noted that although the increase of incidence angle will reduce the SNR and result in a decrease in current measurement accuracy, the SNR will also increase with the decrease of flight height or the increase of wind speed. Therefore, for a designed system, the obtained data may have the same SNR due to the adjustment of flight height or the change of wind speed.

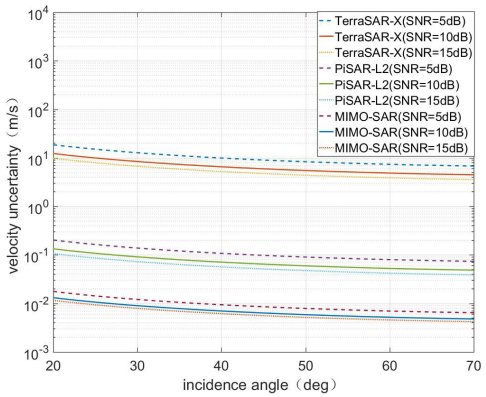

(a)

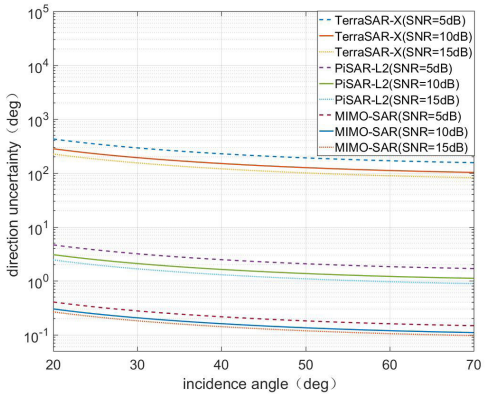

(b)

FIGURE 4. The accuracy of current vector varies with incidence angle. (a) Change of velocity measurement accuracy. (b) Change of direction measurement accuracy.

When faced with data selection with the same SNR, the simulation results show that the better current measurement result can be obtained by processing data with the large incidence angle. Of course, at the same incidence angle, when the SNR changes due to wind speed and altitude, the current accuracy will also change, that is, higher wind speed and lower flight height will make the SNR and accuracy higher.

Figure 5 (a) and (b) respectively represent the simulation results of current velocity and direction accuracy with the sub-aperture squint angle. The results show that under the same SNR, the larger the sub-aperture squint angle, the higher the accuracy of the current vector measurement. In addition, the MIMO-SAR results are the best, PiSAR-L2 is the second, and TerraSAR-X is the worst. The sub-aperture squint angle is related to the azimuth beam width of the signal. Since the beam width of the spaceborne system is generally lower than the parameters of the airborne radar, the TerraSAR-X has the lowest accuracy in all simulation results.

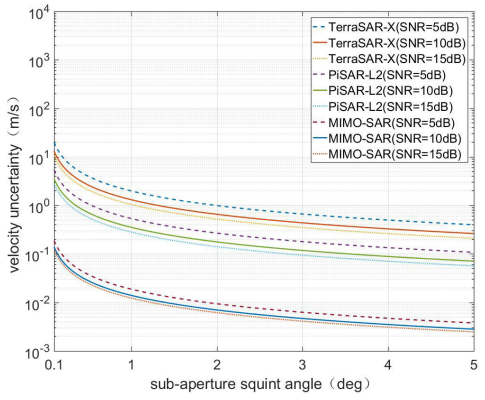

(a)

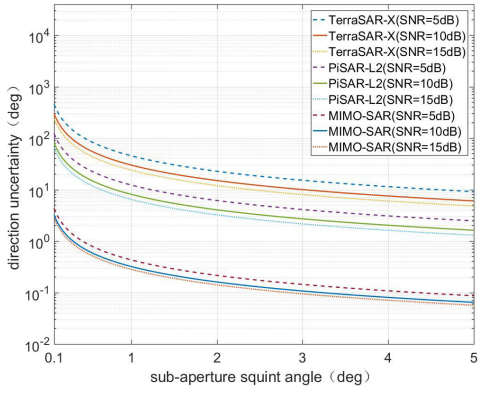

(b)

FIGURE 5. The accuracy of current vector varies with sub-aperture squint angle. (a) Change of velocity measurement accuracy. (b) Change of direction measurement accuracy.

The above simulation results are under the condition of 1km current field spatial resolution, but in reality, the airborne data swath is far less than the spaceborne data swath, and it is one of the advantages of airborne data to obtain

relative fine-scale current variations. Therefore, in order to meet the practical application, the simulation results of airborne parameters under the condition of current field resolution within 100 meters should be considered. Figure 6 shows the variation of the vector measurement accuracy with the spatial resolution of the current field obtained from the simulation of two sets of airborne parameters, indicating that the accuracy decreases with the decrease of the current field resolution cell. From Figure 6 (a), when the SNR is 10dB, the MIMO-SAR system can achieve a velocity measurement accuracy of 0.1m/s at a spatial resolution of 70m, corresponding to the direction measurement accuracy of 2° in Figure 6 (b). However, the accuracy of PiSAR-L2 system is only 0.7m/s and 16.2° at 100m current field resolution. Therefore, from the perspective of practical application, MIMO-SAR data is more suitable for MA-ATI processing. The following airborne parameter simulations are discussed under the condition of 100m current field resolution.

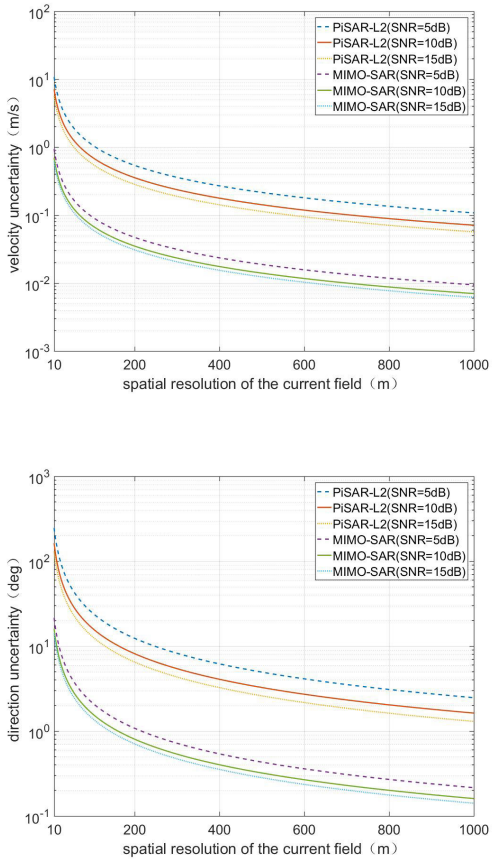

FIGURE 6. The accuracy of current vector varies with the spatial resolution of current field under airborne parameters. (a) Change of velocity measurement accuracy. (b) Change of direction measurement accuracy.

Based on the above analysis, it can be seen that in the actual data processing with MA-ATI technology, the high-resolution MIMO-SAR airborne experimental data should be selected, and the current measurement accuracy is the highest in the case of the optimal baseline length, larger incidence angle and larger azimuth beam width. Under the three fixed parameter simulation conditions shown in Table 1, the velocity and direction accuracy are shown in Table 2. Note that TerraSAR-X current direction accuracy measurements are large and have no practical significance.

TABLE 2. Simulation results of current vector measurement accuracy (5dB/10dB/15dB SNR).

Parameters	PiSAR-L2	MIMO-SAR	TerraSAR-X	Unit
velocity accuracy	1.1/0.7/0.5	0.09/0.07/0.06	9.9/6.5/5.2	m/s
direction accuracy	25/16/13	2.2/1.6/1.4	228/150/120	deg

B. ANALYSIS OF THE INFLUENCE OF CURRENT PARAMETERS ON THE CURRENT ACCURACY

The above discussion is based on the current measurement with a fixed velocity and direction, but in the actual marine environment, the current vectors often change. Therefore, this article further studies the influence of different current parameters on the measurement accuracy of MA-ATI under the condition of fixed radar parameters (10dB SNR). The simulation current velocity is set in the range of 0.1 $\sim$ 2m/s, and the direction is set in the range of 0 $\sim$ 90°. According to the analysis of accuracy in Section II-B, it can be known that the current velocity and direction will only affect direction measurement accuracy.

Figure 7 (a) shows the effect of current velocity on the direction accuracy when the direction is 45°. It can be seen that as the velocity increases, the direction result is more accurate. In the variable velocity range, the direction measurement accuracy of MIMO-SAR varies from 1.4° to 28.4°. Figure 7 (b) shows the effect of current direction on the direction accuracy when the current velocity is 1.77m/s. The closer the current direction is to zero, that is, the closer to the azimuth direction, the higher the direction measurement accuracy. This conclusion can also be explained by the principle of MA-ATI. According to (4), the azimuth velocity is related to the difference between the forward and backward velocity components. Therefore, when the current direction is close to the azimuth direction, the difference between the forward and backward velocity becomes larger, which is conducive to obtaining more accurate azimuth velocity, and the current direction will be more accurate. At this time, the direction measurement accuracy range of MIMO-SAR is 0.08° $\sim$ 2.3°, and that of PiSAR-L2 is 2° $\sim$ 22.9°. In other cases of different velocities and directions, it has the same changing law.

In the actual marine environment, the complex changes of wind wave and ocean current will make SAR imaging appear nonlinear, resulting in azimuth velocity migration. Azimuthal migration will make the velocity of different scatterers stack, and then produce distortion. However, according to the analysis of Sletten [29], this kind of distortion mainly exists in the place where the velocity gradient of surface water body is large, such as land river, while the distortion caused by ocean phenomenon is relatively small. More-

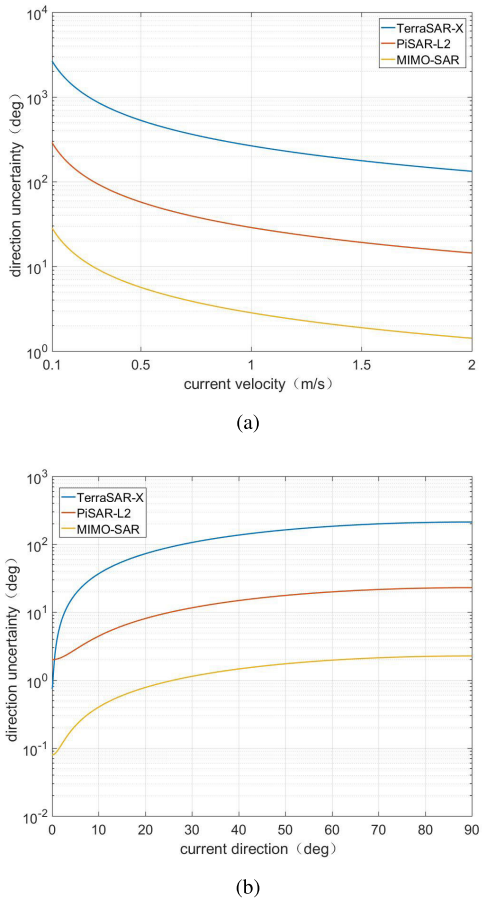

FIGURE 7. Influence of the current velocity and direction on direction measurement accuracy. (a) Changes of current direction accuracy with the velocity. (b) Changes of current direction accuracy with the direction.

over, in data processing, multi-look processing can further reduce the impact of large-scale wave orbital velocity. For example, Romeiser *et al.* [19] Obtained better current field results through multi-look processing. Therefore, we believe that the simulation results in this article are of practical significance.

In order to obtain the numerical change of direction accuracy under more velocity and direction conditions, Table 3 shows the discrete numerical results obtained by simulation with MIMO-SAR parameters at 10dB SNR. It shows that the measurement accuracy of different current directions can be better than 10 degrees when the current velocity is greater than 0.5 m/s.

TABLE 3. Direction accuracy of the current in MIMO-SAR parameter simulation.

Velocity/Direction	0°	20°	40°	60°	80°	90°
0.1m/s	1.4°	13.8°	25.8°	34.7°	39.5°	40°
0.5m/s	0.3°	2.8°	5.2°	7°	7.9°	8°
1.0m/s	0.1°	1.4°	2.6°	3.5°	3.9°	4°
1.5m/s	0.09°	0.9°	1.7°	2.3°	2.6°	2.7°
2.0m/s	0.07°	0.7°	1.3°	1.7°	2°	2°

IV. SIMULATION ANALYSIS OF CURRENT VECTOR MEASUREMENT ERROR

A. ANALYSIS OF THE INFLUENCE OF WIND FIELD PARAMETERS ON CURRENT ERROR

The wind field parameters include wind speed and wind direction. The change in wind speed mainly causes the change of ocean surface roughness, which changes the signal-to-noise ratio of the ocean surface echo signal and the change of coherence coefficient, which in turn affects the accuracy of the current measurement, but the literature [20] has shown that the dependence of ATI signal on wind speed is not obvious under moderate wind speed conditions, so this article does not discuss in detail the influence of wind speed on the experimental results. According to the analysis in Section II-C, the current measurement error caused by the net Bragg wave phase velocity is mainly affected by the change of wind direction, so the following will study the variation of current measurement error with wind direction through simulation. The MIMO-SAR radar parameters shown in Table 1 are used in the simulation.

According to (25) and (26), the forward and backward velocity component errors vary with the wind direction, as shown in Figure 8 (a), where the 0 degree represents the wind moving close to the radar along the range direction, and the 180 degree represents the wind moving away from the radar. The results in the figure show that when the horizontal axis is ±90°, which represents the wind direction is perpendicular to the range direction, the error slope and difference between the two velocity components are the largest. When the horizontal axis is near 0 and 180 degrees, which represents the wind direction is parallel to the range direction, the errors of the two components are the same. According to (27), the results of Figure 8 (a) will affect the azimuth velocity component error. Figure 8 (b) shows the simulation result of the azimuth velocity component error ε_{u_a} represented by the blue line and the range velocity component error ε_{u_r} represented by the red line with the wind direction. The results of Figure 8 (b) show that when the wind direction is parallel to the range direction, the range velocity component error is the largest and the azimuth velocity component error is the smallest. When the wind direction is perpendicular to the range direction, the range velocity component error is the smallest, and the azimuth velocity component error is the largest, and a small change of wind direction will cause significant error changes in both velocity components. The variation law of the azimuth velocity component error is consistent with that of the difference between the two lines in Figure 8 (a), and the error value is related to the sub-aperture squint angle. The larger the sub-aperture squint angle, the smaller the azimuth velocity component error. In the whole range of wind directions, the maximum error of the azimuth velocity component is 0.84m/s, and the maximum error of the range velocity component is 0.28m/s.

When the SAR radar beam illuminates the ocean surface current with a velocity of 1.25m/s and a direction of 45°,

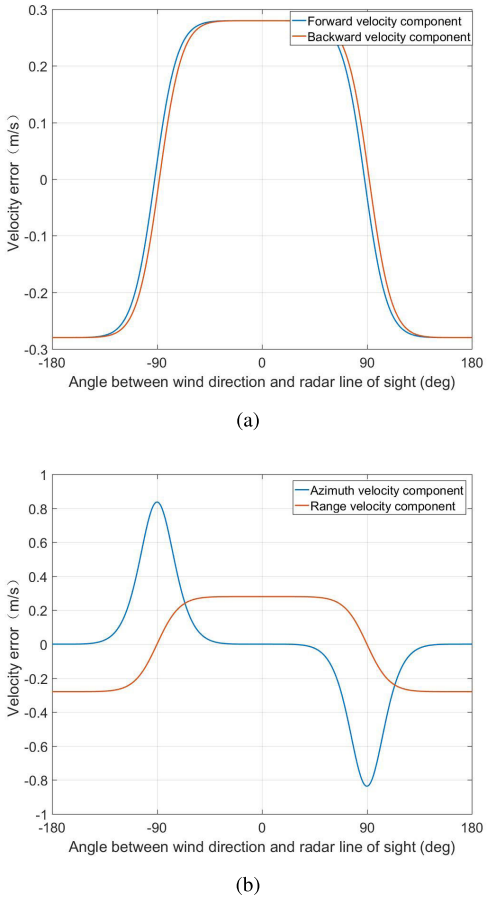

FIGURE 8. Error changes of different velocity components caused by wind direction. (a) Change of forward and backward velocity component errors. (b) Change of azimuth and range velocity component errors.

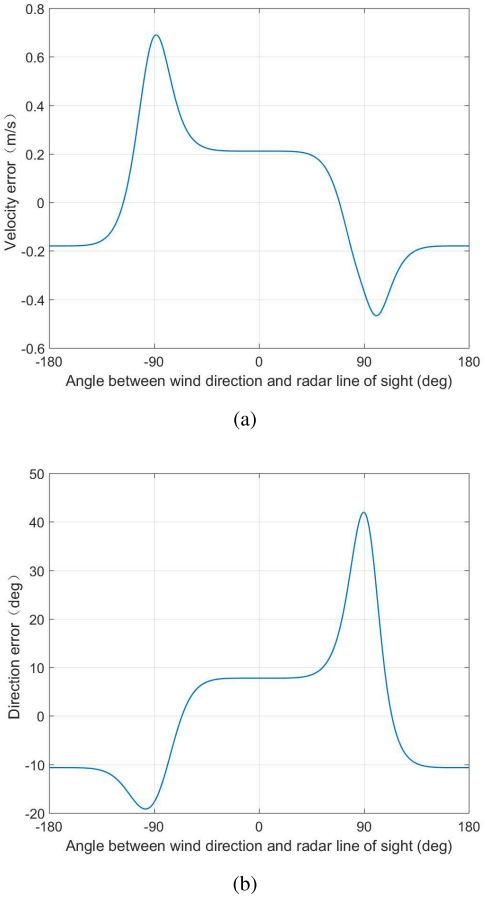

FIGURE 9. Influence of the wind direction on current vector error. (a) Current velocity error varies with wind direction. (b) Current direction error varies with wind direction.

according to (28) and (29), it can be obtained that the current vector error varies with the wind direction. Figure 9 (a) shows the variation of the current velocity error with the wind direction. When the angle between the wind direction and the radar line of sight is -90°, the maximum error is 0.69m/s. Figure 9 (b) shows the current direction error with the wind direction. When the angle between the wind direction and the radar line of sight is 90°, the maximum error is 42°. The simulation results show that in the actual data processing of MA-ATI, the current vector results obtained without processing the Bragg phase velocity error are difficult to represent the real current, so it is necessary to correct the current measurement errors in the forward and backward sub-aperture data before calculating the current vector with MA-ATI.

B. SIMULATION OF CURRENT MEASUREMENT ERROR CORRECTION

In order to reduce the influence of the net Bragg wave phase velocity on the MA-ATI current measurement results, it is necessary to combine the existing methods to eliminate the influence of wave motion. Graber *et al.* gave two methods to correct the current measurement error in the literature [30]: one requires known wind and wave information, combined with a microwave scattering model to calculate wave motion; the other is to use discrete actual current data to calibrate the measurement results. The current data corrected by these two methods are basically the same as the current data obtained by shore-based HF radar, but accurate prior information is not easy to obtain synchronously. In 2003, Kim *et al.* proposed a method to eliminate the net Bragg wave phase velocity using L and C dual-band along-track interferometric SAR data [31], which does not require wind direction information, but there are fewer SAR platforms that meet the experimental conditions. Romeiser and Thompson [20] and Romeiser [32] used the established along-track interferometric SAR imaging simulation model to reduce the errors through an iterative correction method, which reduces the dependence on prior information, improves the calculation efficiency, and is a commonly used current correction method.

The imaging model used in the iterative correction method is called M4S, which was developed by Roland Romeiser of the University of Hamburg, and is based on the improved composite sea surface model to numerically simulate the

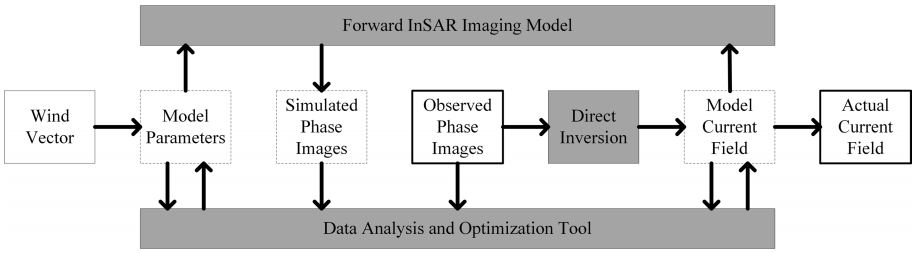

FIGURE 10. Schematic diagram of iterative current inversion [32].

characteristics of the ocean surface current [20], [33], [34]. Reference [32] gives the basic concept of iterative current inversion of along-track interferometric SAR based on the M4S model, as shown in Figure 10, where the specific process of current correction can be found in reference [35]. The experimental results in [35] show that the M4S iterative calculation method can reduce the errors caused by the wind field to within 0.06m/s. Therefore, this article considers that the iterative method can be combined with MA-ATI to correct the vector measurement error of the current field. In the specific process, the M4S iterative method is used to correct the current components in the forward and backward sub-aperture data, and then the velocity and direction of the current are calculated according to the geometric relationship. In this article article article, we did not process the actual data, so we did not use the M4S simulation SAR image to realize the correction process. However, in order to illustrate the effect of the proposed correction method, the variations of current errors before and after correction are simulated based on formulas.

Firstly, according to the simulation and analysis process in Section IV-A, the maximum error caused by wind direction under different velocity and direction is obtained, which is expressed as the change of error before iterative correction, as shown in Figure 11. Figure 11 (a) shows the velocity measurement error under different velocity and direction environment. The results show that the greater the current velocity, the closer the direction is to the range, the smaller the error. When the current velocity is 2m/s and the direction is 90°, the minimum error obtained is 0.28m/s. On the contrary, when the velocity is 0.1m/s and the direction is 0°, the maximum error obtained is 0.84m/s. Figure 11 (b) shows the direction measurement error under different current environment, and the error is large under most conditions. Only when the velocity is greater than 1.5m/s and the direction is less than 10°, the current direction error will be less than 10°, and the greater the current velocity, the closer the direction is to the azimuth direction, the smaller the direction error. When the velocity is 2m/s and the direction is 0°, the minimum direction error is 8°, and the maximum direction error indicated by the dark red at the bottom in Figure 11 (b) reaches 180°, which is completely unable to represent the true current direction. Then, it is assumed that the velocity errors ε_{u_f} and ε_{u_b} in the forward and backward directions and

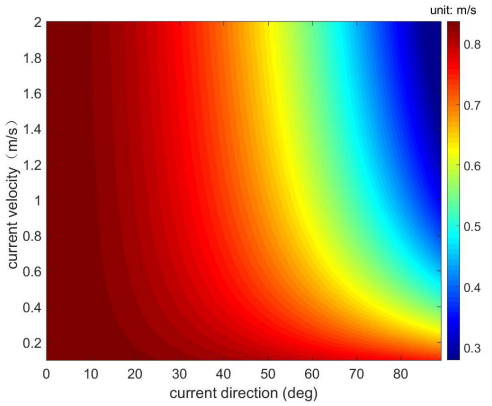

(a)

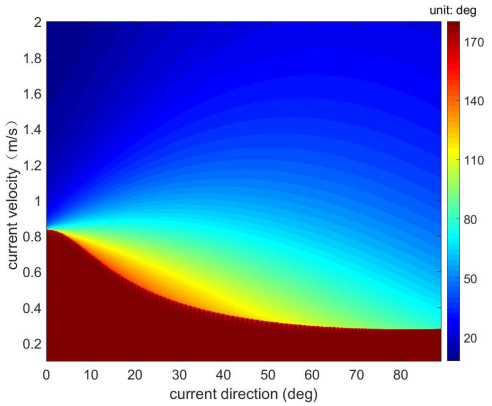

(b)

FIGURE 11. Change of current vector measurement error before correction. (a) Velocity error of different current environment. (b) Direction error of different current environment.

ε_{u_r} in the range direction can reach 0.06m/s after iterative correction, which conform to the experimental results in the literature [35]. The velocity and direction error results of the current vectors can be obtained by introducing them into (27), (28) and (29), as the change of error after correction, as shown in Figure 12. According to the color scale different from Figure 11, the errors under various current field conditions are significantly reduced and the correction effect is obvious. The change rule of current velocity error in Figure 12 (a) is the same as Figure 11 (a), and the variation range of velocity

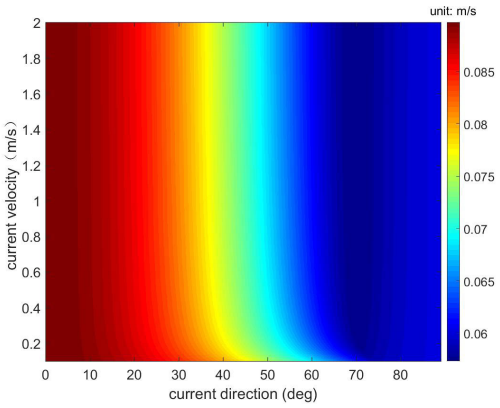

(a)

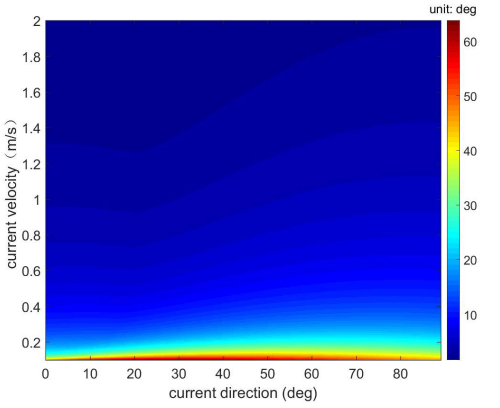

(b)

FIGURE 12. Change of current vector measurement error after correction. (a) Velocity error of different current environment after correction. (b) Direction error of different current environment after correction.

error after correction is reduced to 0.057m/s ∼ 0.09m/s. In the change of current direction error shown in Figure 12 (b), when the observed current velocity reaches more than 0.5m/s, the direction measurement error is reduced to within 10°. Besides, when the velocity is 2m/s and the direction is 0°, the minimum direction error is reduced to 1.7°, and when the velocity is 0.1m/s, the maximum direction error is reduced to 63.8°. For the current conditions discussed in Section IV-A where the velocity is 1.25m/s and the direction is 45°, the vector velocity error is reduced to 0.07m/s and the direction error is reduced to 3.4° after correction.

V. CONCLUSION

MA-ATI is a new method for detecting two-dimensional current field using existing ATI data, but the application effect in actual data is not clear. In this article, the accuracy and error model of MA-ATI is deduced and calculated theoretically, and the influence of radar parameters such as baseline length, incidence angle, sub-aperture squint angle, and current parameters on the measurement accuracy is simulated. The results show that MA-ATI technology is more suitable for MIMO-SAR airborne data, and the greater the observed current velocity, the closer to the azimuth propagation, the higher the accuracy of the current measurement. The influence of wind direction on the current measurement error is analyzed through simulation, which shows that the measurement results without error correction is difficult to represent the real current. The iterative correction of the sub-aperture net Bragg wave phase velocity before calculating the current vector is necessary, which can effectively reduce the measurement error. The relevant conclusions provide valuable references for improving the application ability of MA-ATI in actual current vector measurement.

REFERENCES

[1] R. M. Goldstein and H. A. Zebker, "Interferometric radar measurement of ocean surface currents," *Nature*, vol. 328, no. 6132, pp. 707–709, Aug. 1987.

[2] G. Farquharson, H. Deng, Y. Goncharenko, and J. Mower, "Dual-beam ATI SAR measurements of surface currents in the nearshore ocean," in *Proc. IEEE Geosci. Remote Sens. Symp.*, Jul. 2014, pp. 2661–2664.

[3] S. J. Frasier and A. J. Camps, "Dual-beam interferometry for ocean surface current vector mapping," *IEEE Trans. Geosci. Remote Sens.*, vol. 39, no. 2, pp. 401–414, 2001.

[4] J. V. Toporkov, D. Perkovic, G. Farquharson, M. A. Sletten, and S. J. Frasier, "Sea surface velocity vector retrieval using dual-beam interferometry: First demonstration," *IEEE Trans. Geosci. Remote Sens.*, vol. 43, no. 11, pp. 2494–2502, Nov. 2005.

[5] J. Marquez, B. Richards, and C. Buck, "Wavemill: A novel instrument for ocean circulation monitoring," in *Proc. Eur. Conf. Synth. Aperture Radar*, 2010, pp. 1–3.

[6] K. Ouchi, T. Yoshida, and C.-S. Yang, "A theory of multiaperture along-track interferometric synthetic aperture radar," *IEEE Geosci. Remote Sens. Lett.*, vol. 16, no. 10, pp. 1565–1569, Oct. 2019.

[7] K. Ouchi, T. Yoshida, and C.-S. Yang, "Multi-aperture along-track interferometric SAR for estimating velocity vector of ocean currents," in *Proc. IEEE Int. Geosci. Remote Sens. Symp. (IGARSS)*, Jul. 2018, pp. 1001–1004.

[8] T. Yoshida, K. Ouchi, and C.-S. Yang, "Validation of MA-ATI SAR theory using numerical simulation for estimating the direction of moving targets and ocean currents," *IEEE Geosci. Remote Sens. Lett.*, early access, Apr. 16, 2020, doi: 10.1109/LGRS.2020.2983160.

[9] K. Ouchi, T. Yoshida, and C.-S. Yang, "Multi-aperture along-track interferometric (MA-ATI) SAR for velocity vector estimation of ocean currents using conventional ATI SAR data," presented at the Int. Symp. Remote Sens., Pyeongchang, South Korea, 2018.

[10] H. S. Jung, Z. Lu, J. S. Won, M. P. Poland, and A. Miklius, "Mapping three-dimensional surface deformation by combining multiple-aperture interferometry and conventional interferometry: Application to the June 2007 eruption of Kilauea Volcano, Hawaii," *IEEE Geosci. Remote Sens. Lett.*, vol. 8, no. 1, pp. 34–38, Jan. 2011.

[11] N. B. D. Bechor and H. A. Zebker, "Measuring two-dimensional movements using a single InSAR pair," *Geophys. Res. Lett.*, vol. 33, no. 16, pp. 275–303, 2006.

[12] S. Wollstadt, P. Lopez-Dekker, F. De Zan, and M. Younis, "Design principles and considerations for spaceborne ATI SAR-based observations of ocean surface velocity vectors," *IEEE Trans. Geosci. Remote Sens.*, vol. 55, no. 8, pp. 4500–4519, Aug. 2017.

[13] M. S. Seymour and I. G. Cumming, "Maximum likelihood estimation for SAR interferometry," in *Proc. IEEE Int. Geosci. Remote Sens. Symp. (IGARSS)*, Aug. 1994, pp. 2272–2275.

[14] H.-S. Jung, J.-S. Won, and S.-W. Kim, "An improvement of the performance of multiple-aperture SAR interferometry (MAI)," *IEEE Trans. Geosci. Remote Sens.*, vol. 47, no. 8, pp. 2859–2869, Aug. 2009.

[15] H.-S. Jung, W.-J. Lee, and L. Zhang, "Theoretical accuracy of along-track displacement measurements from multiple-aperture interferometry (MAI)," *Sensors*, vol. 14, no. 9, pp. 17703–17724, Sep. 2014.

[16] H. Johnsen, V. Nilsen, G. Engen, A. A. Mouche, and F. Collard, "Ocean Doppler anomaly and ocean surface current from sentinel 1 tops mode," in *Proc. IEEE Int. Geosci. Remote Sens. Symp. (IGARSS)*, Jul. 2016, pp. 3993–3996.

[17] D.-J. Kim, W. M. Moon, D. A. Imel, and D. Moller, "Remote sensing of ocean waves and currents using NASA (JPL) AIRSAR along-track interferometry (ATI)," in *Proc. IEEE Int. Geosci. Remote Sens. Symp.*, Jun. 2002, pp. 931–933.
[18] D. Moller, S. J. Frasier, D. L. Porter, and R. E. McIntosh, "Radar-derived interferometric surface currents and their relationship to subsurface current structure," *J. Geophys. Res., Oceans*, vol. 103, no. C6, pp. 12839–12852, Jun. 1998.
[19] R. Romeiser, H. Runge, S. Suchandt, R. Kahle, C. Rossi, and P. S. Bell, "Quality assessment of surface current fields from TerraSAR-X and TanDEM-X along-track interferometry and Doppler centroid analysis," *IEEE Trans. Geosci. Remote Sens.*, vol. 52, no. 5, pp. 2759–2772, May 2014.
[20] R. Romeiser and D. R. Thompson, "Numerical study on the along-track interferometric radar imaging mechanism of oceanic surface currents," *IEEE Trans. Geosci. Remote Sens.*, vol. 38, no. 1, pp. 446–458, Jan. 2000.
[21] W. J. Plant, "Bragg scattering of electromagnetic waves from the air/sea interface," in *Surface Waves and Fluxes*. Cham, Switzerland: Springer, 1990, pp. 41–108.
[22] W. J. Plant, W. C. Keller, and K. Hayes, "Measurement of river surface currents with coherent microwave systems," *IEEE Trans. Geosci. Remote Sens.*, vol. 43, no. 6, pp. 1242–1257, Jun. 2005.
[23] R. B. Thapa, M. Watanabe, M. Shimada, and T. Motohka, "Examining high-resolution PiSAR-L2 textures for estimating tropical forest carbon stocks," *IEEE J. Sel. Topics Appl. Earth Observ. Remote Sens.*, vol. 9, no. 7, pp. 3202–3209, Jul. 2016.
[24] M. Shimada, N. Kawano, M. Watanabe, T. Motooka, and M. Ohki, "Calibration and validation of the Pi-SAR-L2," in *Proc. Asia–Pacific Conf. Synth. Aperture Radar (APSAR)*, 2013, pp. 194–197.
[25] J. Wang, C. Ding, X. Liang, L. Chen, and Z. Qi, "Research outline of airborne MIMO-SAR system with same time-frequency coverage," *J. Radars*, vol. 7, no. 2, pp. 220–234, 2018.
[26] R. Romeiser, "Surface current measurements by spaceborne along-track inSAR–terraSAR-X, tanDEM-X, and future systems," in *Proc. IEEE/OES 11th Current, Waves Turbulence Meas. (CWTM)*, Mar. 2015, pp. 1–4.
[27] R. Romeiser, S. Suchandt, H. Runge, and U. Steinbrecher, "High-resolution current measurements from space with TerraSAR-X along-track InSAR," in *Proc. OCEANS-EUROPE*, May 2009, pp. 1–5.
[28] R. Romeiser, M. Schwäbisch, J. Schulz-Stellenfleth, D. R. Thompson, R. Siegmund, A. Niedermeier, W. Alpers, and S. Lehner, "Study on concepts for radar interferometry from satellites for ocean (and land) applications (KoRIOLiS)," Univ. Hamburg, Hamburg, Germany, Final Rep., 2002. [Online]. Available: http://www.ifm.uni-hamburg.de/~romeiser/koriolis.htm
[29] M. A. Sletten, "An analysis of gradient-induced distortion in ATI-SAR imagery of surface currents," *IEEE Trans. Geosci. Remote Sens.*, vol. 44, no. 7, pp. 1995–2002, Jul. 2006.
[30] H. C. Graber, D. R. Thompson, and R. E. Carande, "Ocean surface features and currents measured with synthetic aperture radar interferometry and HF radar," *J. Geophys. Res., Oceans*, vol. 101, no. C11, pp. 25813–25832, Nov. 1996.
[31] D.-J. Kim, W. M. Moon, D. Moller, and D. A. Imel, "Measurements of ocean surface waves and currents using L- and C-band along-track interferometric SAR," *IEEE Trans. Geosci. Remote Sens.*, vol. 41, no. 12, pp. 2821–2832, Dec. 2003.
[32] R. Romeiser, "Current measurements by airborne along-track InSAR: Measuring technique and experimental results," *IEEE J. Ocean. Eng.*, vol. 30, no. 3, pp. 552–569, Jul. 2005.
[33] R. Romeiser, W. Alpers, and V. Wismann, "An improved composite surface model for the radar backscattering cross section of the ocean surface: 1. theory of the model and optimization/validation by scatterometer data," *J. Geophys. Res., Oceans*, vol. 102, no. C11, pp. 25237–25250, Nov. 1997.
[34] R. Romeiser and W. Alpers, "An improved composite surface model for the radar backscattering cross section of the ocean surface: 2. Model response to surface roughness variations and the radar imaging of underwater bottom topography," *J. Geophys. Res., Oceans*, vol. 102, no. C11, pp. 25251–25267, Nov. 1997.
[35] X.-Z. Yu, J.-S. Chong, and W. Hong, "An iterative method for ocean surface current retrieval by along-track interferometric SAR," *J. Electron. Inf. Technol.*, vol. 34, no. 11, pp. 2660–2665, Jul. 2013.

YAN LI received the B.S. degree in communication engineering from Jilin University, Changchun, China, in 2016. He is currently pursuing the Ph.D. degree with the National Key Laboratory of Microwave Imaging Technology, Chinese Academy of Sciences. His research interests include microwave ocean remote sensing, signal analysis, and information processing.

JINSONG CHONG (Senior Member, IEEE) received the Ph.D. degree from the Chinese Academy of Sciences, Beijing, China, in 2003. She has been with the Institute of Electronics, Chinese Academy of Sciences. Her research interests include target detection and recognition, remote sensing image information processing, and ocean microwave remote sensing.

KAI SUN received the B.S. degree in electronic engineering from Dalian Maritime University, Dalian, China, in 2018. He is currently pursuing the Ph.D. degree with the National Key Laboratory of Microwave Imaging Technology, Chinese Academy of Sciences, Beijing, China. His research interest includes microwave remote sensing of the ocean.

XUE YANG received the B.S. degree in electronic information engineering from Dalian Maritime University, Dalian, China, in 2019. She is currently pursuing the Ph.D. degree with the National Key Laboratory of Microwave Imaging Technology, Chinese Academy of Sciences. Her research interests include radar imaging and information extraction of ocean remote sensing image.

YAWEI ZHAO received the B.S. degree from the School of Information and Control Engineering from the China University of Mining and Technology, Xuzhou, China, in 2017. He is currently pursuing the Ph.D. degree with the National Key Laboratory of Microwave Imaging Technology, Chinese Academy of Sciences. His research interests include radar imaging and radar signal processing.